Full Text View

Volume 32, Issue 12 (December 2002)

**Journal of Physical Oceanography**
Article: pp. 3616–3637 | Abstract | PDF (3.45M)

# Effect of Penetrating Momentum Flux over the Surface Boundary/Mixed Layer in a *z*-Coordinate OGCM of the Tropical Pacific

**Rong-Hua Zhang and Stephen E. Zebiak**

*International Research Institute for Climate Prediction, Lamont-Doherty Earth Observatory, Columbia University, Palisades, New York*

(Manuscript received February 19, 2001, in final form June 25, 2002)

DOI: 10.1175/1520-0485(2002)032<3616:EOPMFO>2.0.CO;2

ABSTRACT

A simple scheme is proposed for penetrating atmospheric momentum flux over the ocean surface boundary layer or mixed layer (BL/ML) and is tested in the *z*-coordinate NOAA/Geophysical Fluid Dynamics Laboratory Modular Ocean Model (MOM 3) for improving its performance. Analogous to the treatment in layered ocean models, wind stress is applied, as a body force, to the entire BL/ML whose depth is calculated from a nonlocal *K*-profile parameterization scheme. The penetrating scheme presents an explicit and effective way to distribute a priori momentum flux throughout the BL/ML that has varying depth in space and time, instead of just over the uppermost model level with fixed thickness. This additional procedure introduces an explicit mechanism that directly relates wind stress to the BL/ML formulation, which in turn controls current and thermal structure in the upper ocean and the interaction with the underlying thermocline. Two penetrating runs, one over the BL and the other over the ML, have similar results that differ systematically from those with the penetration over fixed depths (control run). It is demonstrated that, with coherent and systematic improvements, this penetrating scheme can have significant effects on simulated equatorial ocean currents and thermal structure not only in the surface layer, but also in the thermocline. Besides more reasonable ML depth simulation in the equatorial central basin, there is substantial reduction in the mean offset of simulated isotherm depths and warm bias in the thermocline, due to downward shift of the maximum upwelling zone in the equatorial central Pacific. Consistent with observations, the penetrating scheme realistically reproduces the springtime reversal of the South Equatorial Current and the corresponding surface warming in the central equatorial Pacific, with accompanying surfacing of the Equatorial Undercurrent Current in March–May.

## 1. Introduction

Global climate anomalies are related with anomalous patterns of sea surface temperature (SST) in the equatorial Pacific Ocean. The SST in that region is to large extent controlled by wind-driven ocean dynamics (e.g., Zebiak and Cane 1987). Among processes that are less well represented in current ocean general circulation models (OGCMs) are the surface current/undercurrent structure, equatorial upwelling, thermocline depth, and their seasonal variations in response to external atmospheric forcing.

One of the major shortcomings in current OGCMs is the parameterization of vertical turbulent mixing processes in the upper ocean. Poorly specified turbulent mixing schemes can lead to large deviations in simulated and observed mean climatology and variability. Considerable efforts have thus been devoted to this problem; some sophisticated schemes have been developed for use in OGCMs that can better produce observed current and thermal structure (e.g., Pacanowski and Philander 1981; Rosati and Miyakoda 1988; Blanke and Delecluse 1993; Chen et al. 1994; Large et al. 1994, 2001; Large and Gent 1999). Two approaches are currently common in the modeling community. The first approach, which is often adopted in *z*-coordinate OGCMs, is based on some prescribed or estimated coefficients of vertical viscosity for momentum and of vertical diffusivity for tracers. In so doing, prescribed atmospheric momentum and thermal fluxes are first applied to the topmost model level, which has a fixed thickness; with estimated coefficients, the added external forcing fields are then penetrated vertically down to subsurface levels. The values of these coefficients are therefore critical for proper transfer of turbulent fluxes in the surface layer and further into the thermocline. A potential problem with coefficient-based mixing approach is that the model may not appropriately and effectively partition turbulent momentum and heat fluxes vertically in the upper ocean layer. Some additional procedures are necessary for enhancing the vertical mixing in the tropical Pacific (e.g., Latif et al. 1994).

The second approach is a bulk mixed layer (ML) model (e.g., Kraus and Turner 1967). This is based on observations that most vigorous turbulence occurs near the ocean surface layer in association with atmospheric forcing, characterized by nearly homogeneous vertical distribution of the ocean properties (temperature, salinity, and horizontal velocity). With this approach, the topmost model layer, which has varying depth in space and time, is explicitly treated as a bulk turbulent well-mixed layer over which momentum and heat fluxes are distributed homogeneously in the vertical. This sort of model has been directly embedded in layer-formulated OGCMs (e.g., Chen et al. 1994; Murtugudde et al. 1996; Rothstein et al. 1998). Evidently, the way to partition the fluxes in *z*-coordinate level OGCMs (e.g., Philander et al. 1987; Zhang and Endoh 1992) is very different from that in layered OGCMs that have a bulk mixed layer embedded (e.g., Chen et al. 1994). Recent comparison studies indicate that ocean models have preferential systematic biases, depending on the approach adopted in mixing parameterization (e.g., Janssen and Kattenberg 1993; Stockdale et al. 1993).

Sterl and Kattenberg (1994) have explicitly embedded the Kraus–Turner ML model into a *z*-coordinate OGCM for the Atlantic Ocean, demonstrating a significant improvement in simulating thermal and current structure in regions where the ocean ML formulation is governed by wind stirring. In this formulation and as layered OGCMs including the ML model, the ML depth determines the extent to which atmospheric momentum and heat fluxes can penetrate downward into the subsurface levels. Such a approach introduces an explicit mechanism that directly relates wind stirring to the ML formulation, which in turn controls current and thermal structure in the upper ocean and the interaction with the underlying thermocline. This has been identified as one of major missing processes in *z*-coordinate OGCMs with coefficient-based vertical mixing parameterization.

Significant progress has recently been made in ocean model development and improvement at the Geophysical Fluid Dynamics Laboratory (GFDL) of the National Oceanic and Atmospheric Administration (NOAA) with the new release of the Modular Ocean Model (MOM 3; Pacanowski and Griffies 1998). Some new features in the model include the implementation of a nonlocal *K*-profile parameterization (KPP) scheme for vertical mixing (Large et al. 1994; Large and Gent 1999) and of an explicit free surface (e.g., Zeng et al. 1991; Zhang and Endoh 1992). Although the MOM 3 has been refined substantially, some systematic errors are still present in the simulated ocean circulation and its seasonal variations in the tropical Pacific, including an overestimation of the strength of the westward flowing South Equatorial Current (SEC) in the central Pacific, a diffuse thermocline with a warm bias at depth, and weak seasonal sea surface temperature (SST) variations in the central and eastern equatorial Pacific. These problems are very typical in *z*-coordinate OGCMs and have been known in the modeling community for many years (e.g., Philander et al. 1987; Latif et al. 1994). In this work, we explore the effects of allowing explicit penetration of momentum flux over the entire boundary layer or mixed layer (BL/ML) in the MOM 3. This additional procedure appears to have some significant effect on the simulated ocean circulation. Some preliminary results are presented here, demonstrating a more realistic simulation of the currents and thermal structure and their seasonal variations in the equatorial central Pacific Ocean.

## 2. The MOM 3 and penetrating momentum flux scheme

The ocean model used in this work is the latest version of the GFDL MOM 3 (Pacanowski and Griffies 1998; A. Rosati et al. 2000, personal communication). The model domain covers the tropical Pacific basin from 30°S to 30°N, 124°E to 80°W, with horizontal resolution of 1° latitude by 1° longitude (but 0.33° latitude between 10°S and 10°N). It has 40 vertical levels

with a constant 10-m resolution in the upper 210 m; the model incorporates realistic continents and bottom topography. Advances in the MOM 3 relative to previous versions include aspects of the model's physics, numerics, and parallelization (details of the model configuration and parameters can be found online at mjh/IRI-ARCS">http://www.gfdl.gov/~mjh/IRI-ARCS).

The MOM 3 is coupled to an advective atmospheric boundary model (Seager et al. 1995) for a proper calculation of sea surface heat flux, which permits the feedback of SST on the atmosphere (Murtugudde et al. 1996). Given only solar radiation, cloud cover, and surface winds, air temperature and humidity are first determined by a thermal balance among different processes within the atmospheric boundary layer, surface sensible and latent heat fluxes are then calculated according to conventional bulk formulas. Since the ocean has a direct control on air temperature and humidity away from continents, it is not appropriate to specify these atmospheric variables in calculating heat flux.

Monthly climatological wind stress is from the National Aeronautics and Space Administration Data Assimilation Office (DAO) Special Sensor Microwave Imager (SSM/I) analysis from 1987 to 1996 (Atlas et al. 1996). The datasets used to calculate the heat flux include solar radiation data from Esbensen and Kushnir (1981), cloud data from the Comprehensive Ocean–Atmosphere Data Set (COADS; da Silva et al. 1994), and all other necessary fields from the National Centers for Environmental Prediction reanalyses (Kalnay et al. 1996). The solar radiation is allowed to penetrate downward to the model subsurface levels according to the scheme given by Rosati and Miyakoda (1988). The freshwater flux in the model includes two terms. One term is concerned with the differences in evaporation and precipitation estimated from COADS. The second term is essentially a restoring boundary condition on sea surface salinity, by which the model top-level salinity is restored to the Levitus (1982) seasonally varying climatology with a relaxation time of 10 days.

The vertical mixing in the MOM 3 is based on a nonlocal KPP scheme (e.g., Large et al. 1994; Large and Gent 1999), which provides vertical viscosity and diffusivity coefficients throughout the water column. As in all $z$-coordinate level OGCMs, atmospheric momentum flux is first added *only* at the uppermost model level, which has a constant thickness (10 m in our model). The downward penetration into deeper levels is then parameterized in the model through variable viscosity coefficients for momentum. In order to obtain a realistic mixed layer structure in the surface as observed, the coefficients are adjusted to be very large in the upper model levels, allowing sufficiently strong mixing for homogenous distribution of ocean properties in the vertical. This procedure is commonly adopted in $z$-coordinate OGCMs and may miss some important physical processes associated with the ML formulation due to wind stirring (Sterl and Kattenberg 1994).

As a modification to the MOM 3 vertical mixing formulation, we have introduced a simple penetrating scheme for momentum flux over the entire boundary layer or mixed layer (BL/ML) in the $z$-coordinate model, partially taking into account the effect of the BL/ML formulation on the ocean circulation. In analogy to layered OGCMs (e.g., Chen et al. 1994; Murtugudde et al. 1996; Rothstein et al. 1998), wind stress is applied, as a body force, to the entire BL/ML, mimicking turbulence wind stirring associated with momentum mixing in the upper ocean. By this assumption, the momentum flux is vertically distributed throughout the BL/ML as

$$\tau = \tau_s(1 + z/h),$$

where $h$ is the BL depth or ML depth (BLD/MLD); $z$ is the vertical height from 0 to $-h$; $\tau_s$ is the wind stress prescribed at the sea surface; and $\tau$ is the penetrating momentum flux, which is linear function of $z$ from the sea surface ($z = 0$) to the base of the BL/ML ($z = -h$). The corresponding zonal momentum equation (i.e., $u$) can be symbolically written as (see Rosati and Miyakoda 1988)

$$\partial u/\partial t = F(u) + \partial(k\partial u/\partial z) + \partial\tau/\partial z/\rho, \quad (1)$$

where the first term on the right represents the combination of the advection, Coriolis, pressure gradient, and horizontal diffusion terms; the second term for vertical diffusion; and the third term for penetrated momentum flux within the BL/ML: $k$ is vertical viscosity coefficient, which is estimated by the KPP scheme, and $\rho$ is the mean density of seawater. Note that the boundary condition in (1) should be $k\partial u/\partial z = 0$ at the ocean surface ($z = 0$) because $\tau_s$ is now absorbed in the third term. At each time step, the KPP scheme estimates $k$ and the BLD/MLD; for regions where the BLD/MLD is greater than the thickness of the first model level (10 m), the momentum flux associated with the wind stress is allowed to penetrate downward to the subsurface levels. In the code, this has been expressed as a source term in the momentum equation, adding the penetrated momentum flux on all model levels within the BL/ML.

The original model, initiated from the Levitus (1982) temperature and salinity fields, is integrated for 8 years with the climatological forcing fields, by which time it has an equilibrium seasonal cycle. This will be referred to a control run. The result to be shown below is from the last year of the run.

Figure 1 exhibits the simulated annual mean boundary layer depth and mixed layer depth from the control run; their seasonal variations along the equator are demonstrated in Fig. 2. As discussed by Large et al. (1994), the BLD depends

on the surface forcing and on the oceanic buoyancy and velocity profiles. Essentially, the BLD is a measure of how deep a boundary layer eddy, with the near-surface velocity and buoyancy, can penetrate into the interior stratification before becoming stable in a Richardson number sense, relative to the local velocity and buoyancy. Numerically, it is the shallowest depth at which a bulk Richardson number first exceeds a critical value, 0.3. As shown in Fig. 1a, the BL is characterized by deep zonal tongues in the winter hemisphere along latitudes of 10°–20° and 5°–10°, and by a shallow tongue across the equatorial region. The BLD shows strong seasonality in the extratropics, with shallowest in the summer but deepest in the winter, indicating the important role of surface heating/cooling in the formulation. In the equatorial region, the BL deepens in the summer and shoals in the spring, an indication of the importance of wind stirring in its formulation. The shallowest BL can be seen to form in the eastern equatorial Pacific and western equatorial Pacific (~ 10 m), with relative deeper in the central basin (~ 20–40 m).

In the MOM 3, the MLD is defined as the depth where the buoyancy difference with respect to the surface is equal to 0.03 cm $s^{-2}$ (Large et al. 1994). There are several other possible definitions for the MLD. The absolute values estimated from various definitions can be different but the patterns are quite similar, which can be seen in Figs. 1b and 3b, with the former being buoyancy-based whereas the latter being temperature-based. The MLD based on the temperature criterion (Fig. 3b) is generally greater than that on the buoyancy criterion (Fig. 1b). To see the performance of the MOM 3 in simulating the ML, we show in Fig. 3 the MLD based on the same temperature criterion from the Levitus data (1982) and model simulation. The observed and simulated MLDs have similar spatial patterns but absolute values differ significantly. The model tends to have a deeper ML in most of the tropical region, reflecting too much downward penetration of isotherms associated with a diffuse thermocline and warm bias in the thermocline. In particular, the model MLD reaches values greater than 100 m in the central off-equatorial regions along 5° on both side of the equator (Fig. 3b).

In general, the MLD has a space–time pattern similar to the BLD, but their differences are evident especially in magnitude, with the BL being generally shallower than the ML. In the equatorial region, they differ significantly in the western Pacific Ocean where the MLD is in the range of 50–70 m whereas the BL is much shallower (Fig. 2). In the central and eastern equatorial Pacific, the BL and ML have similar seasonal variations, with shoaling in the spring and deepening in the summer.

Since the BLD/MLD is generally greater than the thickness of the first model level (10 m) in most regions, the proposed scheme can have an effect on the simulated currents and thermal structure in the model. The effect is expected to be larger in the central equatorial region where the BLD or MLD, with prominent seasonal variations, are much greater than the thickness of the first model level. In the eastern equatorial region, the BLD/MLD is comparable to the thickness of the first model level, and the effect is expected to be small.

To assess the impact of the penetrating momentum flux over the BL and ML, another two runs are performed with all other facets of the numerical simulation being exactly the same (referred to the penetrating runs). One run defines the BLD as the penetrating depth at each time step (e.g., Figs. 1a and 2a) while another run defines the MLD as the penetrating depth (e.g., Figs. 1b and 2b). Results from these penetrating runs will be compared to those from the control run, which distributes the momentum flux over a fixed 10-m depth (the first model layer). To further examine the sensitivity to the penetrating depth, two additional runs are conducted with the penetration over fixed 20-m and 40-m depths, respectively.

## 3. Results with the penetration over the BL

In simulations forced by prescribed atmospheric fields, early versions of MOM could reasonably reproduce basic features of observed upper ocean current and thermal structure and their seasonal variations in the tropical Pacific (e.g., Philander et al. 1987). However, in both early and current versions of the model, there are some systematic errors. In the following, we will focus on some of these typical problems in the equatorial Pacific and demonstrate how the proposed penetrating scheme can achieve some significant improvements. Comparative results are given in this section: one for the control run and the other for the penetrating run that allows the explicit penetration of the momentum flux over the BL, whose depth essentially measures the extent to which atmospheric-driven vigorous turbulence at the sea surface can penetrate downward in the vertical (Large et al. 1994).

The penetrating procedure described above actually does not modify the KPP model through the BL depth. Instead, the penetrating scheme directly modifies the vertical distribution of the momentum flux and therefore the vertical profiles of zonal and meridional currents first in the momentum equations. Then, through the KPP model, this may further change the BL depth and the vertical viscosity and diffusivity coefficients. However, the experiments we made in this paper indicate that the latter effects are not significant. The differences in the estimated BL depths between the control and penetrating runs are small (less than 10 m; figures not given). This suggests that the KPP model performance does not change very much in the penetrating run versus the control run.

### *a. Mixed layer depth*

Figure 4a illustrates the simulated MLD in May from the control run defined as the depth where the buoyancy difference with respect to the surface is equal to 0.03 cm $s^{-2}$. Compared with that estimated from Levitus data (1982) or from layered model simulations with the Kraus–Tuner ML formulation (e.g., Chen et al. 1994; Rothstein et al. 1998), the MOM 3 overestimates the MLD in the most model domains substantially. In particular, the simulated MLD exceeds 80 m in the region from 170°E to 140°W on either sides of the equator, around 2°S and 3°N, respectively. Consequently, isotherm penetration is unrealistically deep in the western and central regions. The penetrating scheme leads to a substantial reduction in the MLD by more than 10 m in most of the interior tropical Pacific (Fig. 4b), with maximum differences of ~ 50 m between the two runs around (2°N, 170°W), which is about 50% of the MLD itself. Similar improvements are evident for other seasons (not shown).

### *b. Currents*

For comparison, Fig. 5 shows observations of zonal currents at 140°W on the equator from the Tropical Ocean and Global Atmosphere (TOGA) Tropical Atmosphere–Ocean Array (TAO) data (e.g., McPhaden 1994). At this site, the SEC/EUC speed and vertical extent undergo large seasonal variations. From August to March, the SEC flows westward; it reverses directions during April–July (i.e., the so-called springtime reversal). The related seasonal variations are evident in the Equatorial Under current. During December and January, the EUC is the weakest, with its core located at depth about 110–140 m; it is stronger and shallower (centered around 80–100 m) in boreal spring, accompanied by its surfacing and the reversed SEC at the surface.

Figure 6a shows sea surface zonal velocity in May that is simulated from the control run. Seasonally, the model surface current speed in the SEC is in the range of 10–60 cm $s^{-1}$ in the central equatorial Pacific. The westward flowing SEC is too strong and extends too deep (see Figs. 7 and 8). A well-known springtime reversal of the SEC (i.e., eastward flow in March–May along the equator) is not captured at all; instead, a westward surface flow is maintained over the entire year. As the trade winds weaken in spring, westward surface currents slow down, but do not reverse direction. This indicates that the model does not appropriately respond to the seasonal variations in the trade winds. The impact of the penetrating momentum flux on the surface zonal current simulation is shown in Fig. 6b. The simulated surface zonal current is now less intense: about 10–20 cm $s^{-1}$ weakening of the SEC in the central basin, more in line with observations from the drifter and TOGA/TAO data (e.g., McPhaden 1994). In particular, associated with the weakened trade winds in the boreal spring, the penetrating model reproduces the reversal of the SEC in the central basin. As observed, the SEC in May flows eastward at speed of 10–20 cm $s^{-1}$ in the central equatorial Pacific (Fig. 6b).

The effects of penetrating momentum flux on the simulations are not limited in the surface layer but extend well into the thermocline. Figures 7 and 8 reveal the differences in the vertical structure of zonal velocity along the equator between the two runs. Comparing with observations from the TOGA/TOA mooring data (Fig. 5), the control run captures the basic features of the SEC/EUC system. For example, the largest EUC core speeds are found in the thermocline, which slopes downward to the west; the EUC has a maximum speed of about 100 cm $s^{-1}$ around 130°W–150°W, with its core depth of about 90 m. Compared to the observations (Fig. 5), however, there are some clear discrepancies, including the strength of the westward flowing SEC, the EUC core speed, and their vertical extent. The most prominent problem in the control run is with the seasonal variations of the SEC/EUC in the central equatorial Pacific. For example, the springtime reversal of the surface currents and the surfacing of the EUC is not reproduced at all in the model (Figs. 7a,c and Fig. 8a). The penetrating run (Figs. 7b,d and 8b) has a much more realistic simulation of the SEC/EUC structure and their seasonal variations. The surfacing of the EUC in March–May is captured quite well, with the springtime reversal of the SEC at the sea surface. In addition, the maximum EUC core speed in the control run is systematically weaker by more than 10% and tends to be slightly farther east and deeper than in the penetrating run (Fig. 8). The penetrating run also captures very well the equatorial intermediate current, a westward flow below the EUC (Fig. 7d). Figure 9a demonstrates more clearly the differences in simulated zonal currents from the two runs at 140°W on the equator, including the strength of the EUC, the depth of the maximum EUC core speed, and the vertical gradient of temperature fields.

Figure 10 shows the seasonal variations of vertical velocity at 140°W on the equator for the two runs. Upwelling associated with the trade winds is a permanent feature in the central and eastern Pacific along the equator, accompanied by downwelling in neighboring latitudes. The upwelling is confined to the upper ocean and does not penetrate below the thermocline. From the two runs, there are some noticeable differences in the simulated upwelling patterns, characterized by a downward shifting of the maximum upwelling zone in the central equatorial Pacific. In the control run (Fig. 10a), the maximum upwelling region tends to be located at a depth shallower than 40 m, whereas the upwelling velocity in the penetrating run has a maximum band at a depth below 40 m (Fig. 10b). In the thermocline depth between 50 and 150 m, the upwelling is substantially enhanced in the penetrating run, in which the contour value at a depth of 100 m is mostly over 200 cm $day^{-1}$ while it is mostly under 200 cm $day^{-1}$ in the control run. Another striking difference is the seasonally varying pattern of the upwelling. Associated with the seasonal cycle of the trade winds (Fig. 10c), it is expected that the upwelling should be weaker during the period of weak southeast trade winds in spring but stronger during summer and fall due to the intensification of the trade winds. The penetrating run captures this seasonal variations well, with the weakened

upwelling in the spring. In the control run, however, a phase lag can be clearly seen (Fig. 10a). While the zonal winds are weakest in April–May, the weakest upwelling occurs in July–August. This indicates that the control run model does not realistically represent the upwelling response to the seasonal variations in the trade winds in the equatorial central Pacific. The apparently different upwelling patterns in the two runs will have an effect on the simulation of upper ocean thermal structure examined below.

### *c. Temperature*

Although no direct modification is made to thermodynamic equations that calculate tracer fields (temperature and salinity), the penetrating scheme has large effects on the thermal structure as well. Figure 11 shows seasonal variations in temperature on the equator at 140°W for the two runs; Fig. 9b gives the vertical profiles of temperature at 140°W on the equator. As is typical in *z*-coordinate OGCMs, the model suffers from some well-known problems. For example, model isotherms extend too deep in the western and central equatorial regions, with a mean offset of more than 20 m relative to corresponding observations (e.g., Levitus 1982; McPhaden 1994). This is accompanied by a systematic warm bias in the thermocline and a cold bias in the near-surface layer, giving rise to a weak and diffuse thermocline. With the penetrating scheme, the improvements are evident (Fig. 11b). The SST differences between the two runs are relatively small; larger differences in temperature simulations occur in the thermocline. The most notable improvement is in the reduction of the mean offset in simulated isotherm depths, with a systematic uplifting of the thermocline by ~ 10–20 m in the equatorial region. For example, the annual-mean depths of 20°C (23°C) at 140°W on the equator are about 160 m (116 m) in the control run; they are reduced to about 150 m (101 m). This is apparently associated with the enhanced upwelling at the upper thermocline depth, which causes an upward displacement of isotherms (Fig. 10). Figure 12 further shows the differences of the simulated annual-mean temperature in the upper 300 m between the two runs. As a result of the uplifted thermocline, the penetrating run has a smaller warm bias in the thermocline than in the control run by ~ 1°C. In addition, the penetrating scheme has significantly enhanced seasonal variability of SST in the central equatorial Pacific (Fig. 11). For example, the simulated annual amplitude of SST in the control run is about 0.8°C (from a warming of ~ 0.3°C in the spring to a cooling of ~ 0.5°C in the fall); it is more than doubled (1.7°C) in the penetrating run (from a warming of ~ 0.8°C in the spring to a cooling of ~ 0.9°C in the fall).

### *d. The heat budget*

The heat budget analyses in the two runs show some differences in various terms of the temperature equation. The penetrating scheme mostly affects zonal and vertical advection in the equatorial central Pacific where the upwelling tends to cool off the surface layer while zonal advection associated with the EUC tends to warm the upper thermocline. Figures 13 and 14 illustrate the seasonal variations in the zonal and vertical advection at 140°W on the equator. In the central equatorial Pacific, zonal advection has a large annual cycle and plays an important role in modulating the upper ocean temperature structure. At the sea surface, it is a cooling term during most of the year because the SEC brings cool water westward; as the trade winds weaken in the spring, it becomes a warming contribution to SST in the late spring and early summer when the surface current reverses toward the east. The penetrating run tends to have the weaker SEC in the central equatorial Pacific, which reduces excessive westward advection of cold water from the east along the equator. In particular, the SEC reversal in the spring brings warm water from the west, contributing to the generation of warming in SST (Fig. 13b). This feature is absent in the control run (Fig. 13a). In the upper thermocline, the stronger EUC in the penetrating run corresponds to the larger magnitude of the positive zonal advection of heat transported from the west.

Another important term to the heat budget in the central equatorial Pacific is the vertical advection. It is a cooling term throughout the year because the upwelling brings cool water upward to the surface layer, being responsible for the existence of the cold tongue of SST. As we have seen, both upwelling velocity and temperature fields in the upper thermocline, which determines the strength of the vertical advection, can be affected by the penetrating scheme. The penetrating run tends to enhance the upwelling in the upper thermocline at depth between 50 and 150 m (Fig. 10b). This corresponds to the increased magnitude of negative vertical advection in the upper thermocline at these depths (Fig. 14b), as compared with the control run (Fig. 14a). This contributes to the colder temperature in the thermocline and helps to reduce the warm bias present in the control run as we have discussed above.

## 4. Results with the penetration over the ML

The results with penetrating momentum flux over the ML are very similar to those over the BL. Even in the western equatorial Pacific where there are large differences in the annual mean depth of the BL and ML and their seasonal variations (Figs. 1–2), the differences in the simulated current and thermal structure between the two penetrating runs are not very large. We will, therefore, not give detailed comparisons here. As an example, Fig. 15 demonstrates seasonal variations in zonal velocity and temperature on the equator at 140°W, which are obtained in a run that allows the penetration of the momentum flux over the ML. Essentially, we have similar improvements observed in section 3 where the momentum flux is allowed to penetrate over the BL, characterized by the springtime reversal of the SEC, the corresponding surface warming in spring, and the seasonal variations in the EUC core speed and the vertical extent.

## 5. Further experiments with the penetration over fixed depths

Since the penetrating depths based on BLD/MLD are much greater than the thickness of the first model level (10 m), the penetrating scheme can directly distribute the momentum flux into the subsurface levels within the BL/ML. As demonstrated, there are significant effects on the simulated ocean circulation in the central equatorial Pacific where the BLD or MLD have large seasonal variations ranging from 10 to 40 m. One possible explanation for such large effects is that in the control run the first model level thickness, fixed to 10 m over which the prescribed atmospheric fluxes are deposited, may be too shallow, so the coefficient-based mixing scheme does not appropriately penetrate the turbulent momentum downward in association with wind stirring. To further examine the sensitivity to penetrating depth, two additional runs are performed in which the momentum flux is allowed to penetrate over the fixed 20-m and 40-m depths, respectively. Figure 16 shows seasonal variations in zonal velocity on the equator at 140°W from these two fixed-depth penetrating runs. In the central equatorial Pacific, the simulated current structure and its seasonal variation have apparent problems similar to the control run. The model EUC core depth is too deep with weak seasonal variations in magnitude and vertical extent; the surface westward flows on the equator (i.e., the SEC) are too strong; the surfacing of the EUC and springtime reversal of the SEC is completely missing in the spring. These experiments suggest that *simple* deeper penetration of the momentum flux over fixed depths does not contribute to the improvements seen in the penetrating runs. The point here is that penetration should be allowed over varying depths in time so that a *z*-coordinate OGCM can have an explicit mechanism that directly relates wind stirring to the BL/ML formulation through changes in its depth.

## 6. Discussion and conclusions

As evident from other modeling experiments and from this study, SST in the equatorial Pacific is determined by various physical processes presented in ocean models, including the SEC/EUC, equatorial upwelling, mixed layer, and thermocline depth. These processes are extremely sensitive to the parameterization of vertical turbulent mixing in the upper ocean. Further progress in ocean modeling and coupled climate prediction critically depends on vertical mixing schemes that are able to realistically reproduce upper ocean current and thermal structure. Part of the challenge is to parameterize different mixing processes that exist in the real ocean and that have enormous variations in mixing strength over a very small depth range: from almost perfect effectiveness in a mixed layer, to something much less in the thermocline, and to almost vanishing small intensity in the deep ocean. It is not surprising that this has proved so difficult to accomplish with a single framework. Undoubtedly, further improvements and better resolved models will be developed over time.

In this study, we explore a simple penetrating scheme for momentum flux over the BL/ML in a *z*-coordinate OGCM. This is based on the observational fact that a well-defined surface BL/ML exists almost everywhere in the World Ocean due to vigorous turbulence by wind stirring associated with momentum mixing. To mimic this phenomenon, the well-known bulk mixed layer model was formulated (i.e., Kraus and Turner 1967) and has been embedded into layered OGCMs (e.g., Chen et al. 1994). In these models, the MLD not only represents the strength of turbulence mixing associated with wind stirring and buoyancy forcing, but also controls the depth over which the incoming momentum and heat fluxes are distributed homogeneously in the vertical. Due to the explicit functional relationships with the local MLD, wind stress additionally has direct effects on the ocean current and thermal structure (e.g., Chen et al. 1994; Rothstein et al. 1998). In the present study, these basic ideas are adopted in the context of the *z*-coordinate MOM 3. Specifically, wind stress is applied as a body force to the entire BL/ML, which has varying depth in space and time, instead of just being applied to the uppermost model level with fixed thickness. In the original MOM 3, the BLD/MLD is a diagnostic variable from the KPP scheme and then the calculated vertical viscosity and diffusivity coefficients depend crucially on the BLD. In the penetrating scheme, as in layered OGCMs, the BLD/MLD can further have an important dynamic and thermodynamic impact on the upper ocean circulation, determining the effective depth over which the momentum flux is distributed in the vertical. Several parallel runs indicate that this simple penetrating scheme has a significant effect on the equatorial current and thermal structure in the tropical Pacific Ocean. Systematic and consistent improvements are obtained over significant portions of the central equatorial Pacific, with a more realistic EUC/SEC structure and temperature field in the near-surface layer and in the thermocline. Model results with and without allowing the explicit penetration of the momentum flux have differences in the simulated equatorial current and thermal fields that can be larger than those caused by ocean models with different vertical mixing schemes (e.g., Large and Gent 1999). Moreover, this scheme can be very easily implemented in any *z*-coordinate OGCM, without additional computational cost.

The results can be qualitatively understood as follows. In the control run, atmospheric momentum input is deposited *entirely* in the topmost model level (5 m); correspondingly large Ekman flow is concentrated immediately on the uppermost layer (10 m thick). With the momentum flux distributed over the entire BL/ML which has varying thickness (generally much deeper than 10 m; see Fig. 1), the Ekman flow now occurs explicitly at each model level within the BL/ML. Along the equator, for example, the applied westward momentum flux associated with the easterly trade winds is distributed over the entire BL/ML; the associated Ekman divergence occurs throughout all model levels within the BL/ML. Thus, the direct effect is to reduce the amplitude of the Ekman divergence in the first model level and to partition part of it to subsurface model levels. As such, the modified penetrating momentum scheme can extend Ekman divergence to deeper depths, where upwelling can now be directly induced. This tends to force isotherms to move upward in the upper thermocline, which helps

to reduce the mean offsets of isotherm depths and warm bias in the thermocline. The uplifted isotherms in the central equatorial Pacific between 150° and 120°W enhance the zonal slope of the isotherms along the equator, having a large eastward zonal pressure gradient along the equator and increasing the strength of the EUC. Due to the penetration into the subsurface layer, the added westward momentum flux associated with the trade winds is reduced in the first model level, as is the intensity of the westward SEC in the central equatorial Pacific.

The improved SEC/EUC structure can directly lead to improved seasonal variations in SST in the central equatorial Pacific where a tongue of cold surface waters prevails throughout the year. For example, in that region zonal advection has a large annual cycle and plays an important role in modulating SST. It is a cooling term during most of the year because the SEC brings cool water westward; as the trade winds weaken in the spring, it becomes a warming contribution to SST in the late spring and early summer when the surface current reverses toward the east. The penetrating runs tend to have a weaker SEC in the central equatorial Pacific, which reduces excessive westward advection of cold water from the east along the equator. Moreover, the SEC reversal in spring brings warm water from the west, contributing to the generation of warming in SST. The stronger EUC in the penetrating runs also contribute to warmer SST in spring due to the increase in advection of heat from the west. Another important factor influencing SST in the central equatorial Pacific is the thermocline depth at which cold water is brought to the surface by vigorous upwelling. As we have seen, the penetrating scheme can affect both the *pattern* of the upwelling and the *temperature* of the thermocline water, with a shallower thermocline depth and stronger vertical temperature gradient between the 15° and 20°C isotherms as compared with the control run. Consequently, the changes in thermocline depth can more easily affect SST. These improvements in the SEC/EUC system, the equatorial upwelling, and thermocline depth all benefit the SST simulation in the model.

The experiments described here represent preliminary attempts to improve MOM 3 performance. Further refinement and extension are under way. It is well known that simulated equatorial circulations are very sensitive to the prescribed wind forcing fields. The results from the control run may not compare well with the TOGA/TAO observations because the forcing may be wrong, not because the ocean physics is wrong (e.g., Large and Gent 1999). Thus, the sensitivity of the control and penetrating runs to different wind stress fields needs to be examined to understand the relative contributions of those factors to model errors and their improvements. Even with the penetrating scheme, the simulated current structure and its seasonal variation are still problematic in the far eastern equatorial Pacific. This can be expected because in that region, the BLD/MLD estimated by the KPP scheme, with little seasonal variation, is comparable to the first model level thickness (10 m). However, the MLD estimated from observations (e.g., Levitus 1982) or from the Kraus–Turner bulk model shows larger seasonal variations. An optimal choice for the penetrating depth should be tested for improving model performance in the eastern equatorial Pacific. Furthermore, we have tested a similar penetrating scheme for heat flux in the *z*-coordinate MOM 3. It turns out that, through changes in the BLD/MLD, this can also improve model simulation of SST and its seasonal variations particularly in the eastern equatorial Pacific, a point previously proposed by Chen et al. (1994). By taking into account these different penetrating schemes for momentum and heat fluxes over the entire BL/ML in the MOM 3, it appears that significant improvements can be made in simulating the mean ocean climatology and seasonal variations. The improved climatology is expected to improve interannual variability associated with El Niño in the tropical Pacific Ocean, characterized by an aperiodic warming of the surface water of the equatorial Pacific every 3–7 years. These ultimately will be tested in a full coupled model.

*Acknowledgments*

We are deeply indebted to A. Rosati, M. Harrison, V. Balaji, R. Pacanowski, and others at GFDL/NOAA for their help and numerous support in setting up the GFDL MOM 3 at the IRI. We would like to thank P. R. Gent, W. G. Large, D. Chen, P. Chang, D. DeWitt, M. Tippett, T. Kagimoto, and reviewers for their helpful comments. This research is supported by the IRI and its sponsors.

---

## REFERENCES

Atlas R., R. Hoffman, S. Bloom, J. Jusem, and J. Ardizzone, 1996: A multiyear global surface wind velocity dataset using SSM/I wind observations. *Bull. Amer. Meteor. Soc.*, **77**, 869–882. Find this article online

Blanke B., and P. Delecluse, 1993: Variability of the tropical Atlantic Ocean simulated by a general circulation model with two different mixed layer physics. *J. Phys. Oceanogr.*, **23**, 1363–1388. Find this article online

Chen D., L. M. Rothstein, and A. J. Busalacchi, 1994: A hybrid vertical mixing scheme and its application to tropical ocean models. *J. Phys. Oceanogr.*, **24**, 2156–2179. Find this article online

da Silva A. M., C. C. Young, and S. Levitus, 1994: *Anomalies of Heat and Momentum Fluxes*. Vol. 3, *Atlas of Surface Marine Data*, NOAA Atlas Series, NOAA Atlas NESDIS 7, 413 pp.

Esbensen S. K., and Y. Kushnir, 1981: The heat budget of the global ocean: An atlas based on estimates from the surface marine observations. Oregon State University Climate Research Institute Rep. 29, 27 pp.

Janssen G., and A. Kattenberg, 1993: On the role of mixing in a tropical ocean general circulation model. *Ann. Geophys.*, **11**, 1116–1129. Find this article online

Kalnay E., Coauthors, 1996: The NCEP/NCAR 40-Year Reanalysis Project. *Bull. Amer. Meteor. Soc.*, **77**, 437–471. Find this article online

Kraus E. B., and J. S. Turner, 1967: A one-dimensional model of the seasonal thermocline. II: The general theory and its consequence. *Tellus*, **19**, 98–106. Find this article online

Large W. G., and P. R. Gent, 1999: Validation of vertical mixing in an equatorial ocean model using large eddy simulations and observations. *J. Phys. Oceanogr.*, **29**, 449–464. Find this article online

Large W. G., J. C. McWilliams, and S. C. Doney, 1994: Oceanic vertical mixing: A review and a model with a nonlocal boundary layer parameterization. *Rev. Geophys.*, **32**, 363–403. Find this article online

Large W. G., G. Danabasoglu, J. C. McWilliams, P. R. Gent, and F. O. Bryan, 2001: Equatorial circulation of a global ocean climate model with anisotropic horizontal viscosity. *J. Phys. Oceanogr.*, **31**, 518–536. Find this article online

Latif M., T. Stockdale, J. Wolff, G. Burgers, E. Maier-Reimer, M. M. Junge, K. Arpe, and L. Bengtsson, 1994: Climatology and variability in the ECHO coupled GCM. *Tellus*, **46A**, 35–366. Find this article online

Levitus S., 1982: *Climatological Atlas of the World Ocean*. NOAA Prof. Paper No. 13, 173 pp. and 17 microfiche.

McPhaden M. J., 1994: Moored time series measurements. *Eos, Trans. Amer. Geophys. Union*, **71,** 760.

Murtugudde R., R. Seager, and A. B. Busalacchi, 1996: Simulation of the tropical oceans with an ocean GCM coupled to an atmospheric mixed-layer model. *J. Climate*, **9**, 1795–1815. Find this article online

Pacanowski R. C., and S. G. H. Philander, 1981: Parameterization of vertical mixing in numerical models of the tropical oceans. *J. Phys. Oceanogr.*, **7**, 952–956. Find this article online

Pacanowski R. C., and S. M. Griffies, 1998: MOM 3.0 manual. NOAA/Geophysical Fluid Dynamics Laboratory, 700 pp. [Available online at smg/mom/web/guide_parent/guide_parent.html">http://www.gfdl.gov/~ smg/mom/web/guide_parent/guide_parent.html.].

Philander S. G. H., W. J. Hurlin, and A. D. Seigel, 1987: Simulation of the seasonal cycle of the tropical Pacific Ocean. *J. Phys. Oceanogr.*, **17**, 1986–2002. Find this article online

Rosati A., and K. Miyakoda, 1988: A general circulation model for upper ocean simulation. *J. Phys. Oceanogr.*, **18**, 1601–1626. Find this article online

Rothstein L. M., R.-H. Zhang, A. J. Busalacchi, and D. Chen, 1998: A numerical simulation of the mean water pathways in the subtropical and tropical Pacific Ocean. *J. Phys Oceanogr.*, **28**, 322–343. Find this article online

Seager R., M. Blumenthal, and Y. Kushinir, 1995: An advective atmospheric mixed layer model for ocean modeling purposes: Global simulation of surface heat fluxes. *J. Climate*, **8**, 1951–1964. Find this article online

Sterl A., and A. Kattenberg, 1994: Embedding a mixed layer model into an ocean general circulation model of the Atlantic: The importance of surface mixing for heat flux and temperature. *J. Geophys. Res.*, **99**, 14139–14157. Find this article online

Stockdale T., D. Anderson, M. Davey, P. Delecluse, A. Kattenberg, Y. Kitamura, M. Latif, and T. Yamagata, 1993: Intercomparison of tropical ocean GCMs. WRCP-79 and WMO/TD No. 545, 43 pp.

Zebiak S. E., and M. A. Cane, 1987: A model El Nino/Southern Oscillation. *Mon. Wea. Rev.*, **115**, 2262–2278. Find this article online

Zeng Q.-C., X.-H. Zhang, and R.-H. Zhang, 1991: A design of an oceanic-GCM without the rigid-lid approximation and its application to the numerical simulation of the Pacific Ocean circulation. *J. Mar. Syst.*, **1**, 271–292. Find this article online

Zhang R.-H., and M. Endoh, 1992: A free surface general circulation model for the tropical Pacific Ocean. *J. Geophys. Res.*, **97**, 11237–11255. Find this article online

---

## Figures

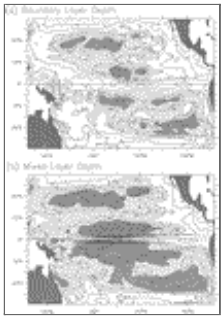

Click on thumbnail for full-sized image.

FIG. 1. The simulated annual-mean (a) boundary layer depth and (b) mixed layer depth from the control run. The BLD is defined as the shallowest depth at which a bulk Richardson number first exceeds a critical value, 0.3; the MLD is defined as the depth where the buoyancy difference with respect to the surface is equal to 0.03 cm $s^{-2}$ [see Large et al. (1994) for more details]. The contour interval is 10 m

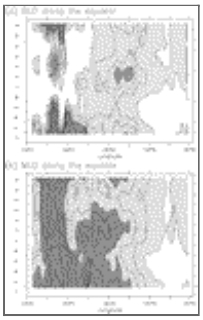

Click on thumbnail for full-sized image.

FIG. 2. Seasonal variations in the simulated (a) BLD and (b) MLD along the equator. The definition of the BLD and MLD is the same as in Fig. 1. The contour interval is 10 m

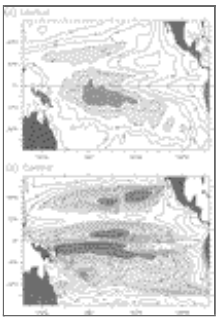

Click on thumbnail for full-sized image.

FIG. 3. Annual-mean mixed layer depth estimated from (a) the Levitus (1982) data and from (b) the model simulation based on temperature criterion as the depth at which the temperature difference from the surface exceeds 0.5°C. The contour interval is 10 m

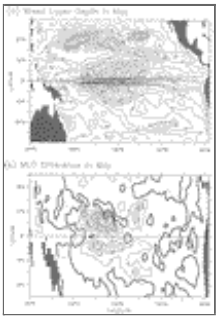

Click on thumbnail for full-sized image.

FIG. 4. Simulated mixed layer depth in May for the (a) control run and (b) its differences relative to the penetrating run over the BL (control − penetrating). The contour interval is 10 m

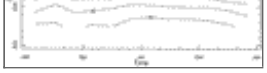

Click on thumbnail for full-sized image.

FIG. 5. Observed climatological mean seasonal cycle of zonal velocity at 0°, 140°W based on 15 years of the TOGA/TAO current meter mooring data from 1984 to 1998. The contour interval is 20 cm $s^{-1}$, with dashed lines for westward flows

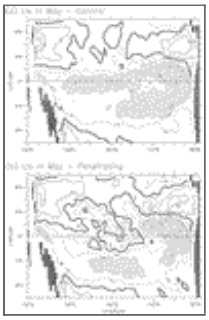

Click on thumbnail for full-sized image.

FIG. 6. Simulated sea surface zonal velocity in May from the (a) control and (b) penetrating runs. The contour interval is 10 cm $s^{-1}$, with dashed lines for westward flows

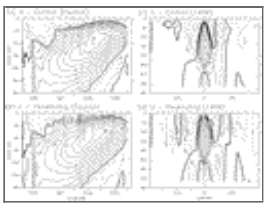

Click on thumbnail for full-sized image.

FIG. 7. (left) Zonal-depth and (right) meridional-depth sections of zonal velocity along (a) (b) the equator and (c) (d) 140°W in May simulated from the (a) (c) control and (b) (d) penetrating runs. The dashed lines are for westward flows with the contour interval being 10 cm $s^{-1}$.

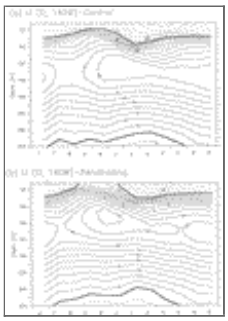

Click on thumbnail for full-sized image.

FIG. 8. Seasonal variations in zonal velocity on the equator at 140°W for the (a) control and (b) penetrating runs. The contour interval is 10 cm $s^{-1}$, with the dashed lines for westward flows

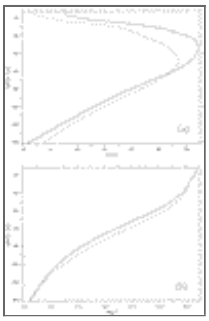

Click on thumbnail for full-sized image.

FIG. 9. The vertical profile of (a) zonal velocity and (b) temperature at 140°W on the equator for May, with the dashed and solid lines for the control and penetrating runs respectively

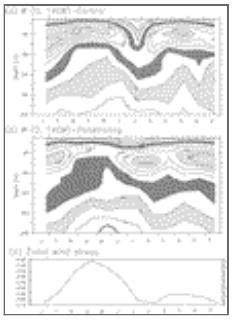

Click on thumbnail for full-sized image.

FIG. 10. Seasonal variations in vertical velocity on the equator at 140°W for the (a) control and (b) penetrating runs and (c) in zonal wind stress (dyn $cm^{-2}$). The contour interval is 50 cm $day^{-1}$ in (a) and (b)

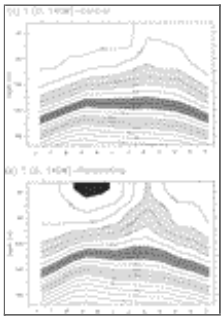

Click on thumbnail for full-sized image.

FIG. 11. As in Fig. 8 but for temperature. The contour interval is 0.5°C

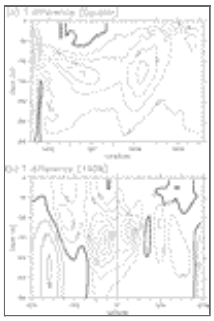

Click on thumbnail for full-sized image.

FIG. 12. The differences of simulated annual-mean temperature in the upper 300 m (a) along the equator and (b) along 140°W between the penetrating and control runs (penetrating − control). The contour interval is 0.2°C

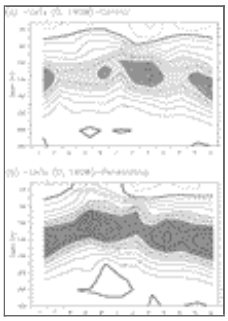

Click on thumbnail for full-sized image.

FIG. 13. Seasonal variations in the zonal advection on the equator at 140°W for the (a) control and (b) penetrating runs. The contour interval is 0.5°C $month^{-1}$, with the dashed lines for negative

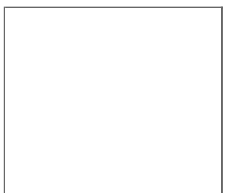

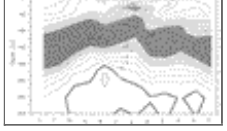

Click on thumbnail for full-sized image.

FIG. 14. Seasonal variations in the vertical advection on the equator at 140°W for the (a) control and (b) penetrating runs. The contour interval is 0.5°C month$^{-1}$, with the dashed lines for negative

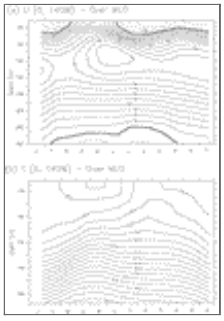

Click on thumbnail for full-sized image.

FIG. 15. Seasonal variations in (a) zonal velocity and (b) temperature on the equator at 140°W for allowing the penetration of the momentum flux over the ML (after 8 years of integration). The contour interval is 10 cm s$^{-1}$ in (a) and 0.5°C in (b) with dashed lines for westward flows

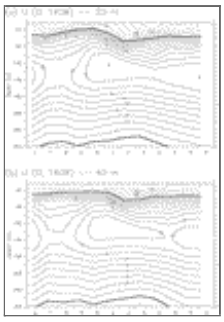

Click on thumbnail for full-sized image.

FIG. 16. Seasonal variations in zonal velocity on the equator at 140°W for allowing the penetration of the momentum flux over fixed (a) 20- and (b) 40-m depths (after 5 years of integration), respectively. The contour interval is 10 cm s$^{-1}$, with the dashed lines for westward flows

*Corresponding author address:* Rong-Hua Zhang, IRI, Lamont-Doherty Earth Observatory, Columbia University, Palisades, NY 10964. E-mail: rzhang@iri.ldeo.columbia.edu

top